Geological and climatic influences on mountain biodiversity

Alexandre Antonelli [1,2,3,4,21]*, W. Daniel Kissling[5,21]*, Suzette G. A. Flantua [5,6,21],
Mauricio A. Bermúdez[7,8,21], Andreas Mulch [9,10], Alexandra N. Muellner-Riehl [11,12], Holger Kreft [13,14],
H. Peter Linder[15], Catherine Badgley [16], Jon Fjeldså[17], Susanne A. Fritz[9,18], Carsten Rahbek[17,19],
Frédéric Herman[20], Henry Hooghiemstra[5] and Carina Hoorn [5,21]*

[1]Gothenburg Global Biodiversity Centre, Göteborg, Sweden. [2]Department of Biological and Environmental Sciences, University of Gothenburg, Göteborg, Sweden. [3]Gothenburg Botanical Garden, Göteborg, Sweden. [4]Department of Organismic and Evolutionary Biology, Harvard University, Cambridge, MA, USA. [5]Institute for Biodiversity and Ecosystem Dynamics, University of Amsterdam, Amsterdam, The Netherlands. [6]Department of Biological Sciences, University of Bergen, Bergen, Norway. [7]Facultad de Ciencias Naturales y Matemáticas, Universidad de Ibagué, Tolima, Colombia. [8]School of Geological Engineering, Sectional Faculty Sogamoso, Pedagogical and Technological University of Colombia, Sogamoso, Colombia. [9]Senckenberg Biodiversity and Climate Research Centre (BiK-F), Frankfurt/Main, Germany. [10]Institute of Geosciences, Goethe University Frankfurt, Frankfurt/Main, Germany. [11]Department of Molecular Evolution and Plant Systematics & Herbarium (LZ), Institute of Biology, Leipzig University, Leipzig, Germany. [12]German Centre for Integrative Biodiversity Research (iDiv) Halle-Jena-Leipzig, Leipzig, Germany. [13]Biodiversity, Macroecology & Biogeography, University of Göttingen, Göttingen, Germany. [14]Centre of Biodiversity and Sustainable Landuse, University of Göttingen, Göttingen, Germany. [15]Department of Systematic and Evolutionary Botany, University of Zurich, Zurich, Switzerland. [16]Department of Ecology & Evolutionary Biology, University of Michigan, Ann Arbor, MI, USA. [17]Center for Macroecology, Evolution and Climate, Natural History Museum of Denmark, University of Copenhagen, Copenhagen, Denmark. [18]Institute of Ecology, Evolution and Diversity, Goethe University Frankfurt, Frankfurt/Main, Germany. [19]Department of Life Sciences, Imperial College London, Silwood Park campus, Ascot, UK. [20]Institute of Earth Surface Dynamics, University of Lausanne, Lausanne, Switzerland. [21]These authors contributed equally: Alexandre Antonelli, W. Daniel Kissling, Suzette G. A. Flantua, Mauricio A. Bermúdez, Carina Hoorn.
*e-mail: alexandre.antonelli@bioenv.gu.se; wdkissling@gmail.com; M.C.Hoorn@uva.nl

Supplementary Discussion

I. Geological and biological discussion of the mountain regions surveyed

Below we provide a brief characterisation of the mountain regions surveyed for this study, further discuss biodiversity patterns and relate our results to previous studies. We cover all regions included in the regional analyses and three additional regions that contributed to the global analyses. The length of these descriptions varies due to differences in the available literature and our research foci.

A) Regions included in the regional analyses (Fig. 3b)

Western North America
Mountain ranges in North America show a strong longitudinal gradient in relief, with a mountainous western region (North American Cordillera; the focus of our analysis) that has been tectonically active since the Cretaceous, mainly through strike slip on the San Andreas fault and extension in the Basin and Range province, with major changes to the landscape over the last 40 Myr[1]. The extensive eastern region (Appalachians; not included in the regional analysis) comprises the craton and the eroded remnants of Palaeozoic orogenies. The Rockies and Front Range in Colorado are currently inactive. The Rockies in Canada show some convergence[2]. Steep bioclimatic gradients between desert basins and rugged mountain ranges characterise the montane and intermontane regions. Coastal ranges along the Pacific capture high levels of precipitation year-round and support some of the highest-biomass forests in the world[3].

Current mountain vertebrate richness (Fig. 1) peaks in the Rocky Mountains, the western edge of the Colorado Plateau, and the southern Sierra Nevada of California. Among the climatic variables, mean annual temperature has the strongest effect on mountain richness (Figs. 3b, S5) and also has a strong relationship with lowland richness. This relationship is positive and linear, in contrast with the asymptotic relationship with annual precipitation. The positive relationship between annual precipitation and richness peaks at c. 600–800 mm/year (Fig. S5a) and may reflect the opposing trends of high amphibian richness in areas of higher rainfall versus high mammal and bird richness in areas of high precipitation seasonality and lower rainfall[5,4,6]. Relief is the strongest geological predictor variable, supplemented by soil heterogeneity, possibly as a result of glaciations in western North America and highly weathered landscapes.

Andes
The Andes reached about half of their current elevation in the middle to late Miocene[7]. This uplift resulted in an orographic barrier that greatly modified South American climate[8,9,10]. The temperature gradient is strongly influenced by the latitudinal south-north orientation of the mountain range and by different climate modes originating in the Pacific and the Atlantic[11]. In

the north, this barrier, enhanced by its concave shape, captures the humid air masses of the Intertropical Convergence Zone and funnels them back into the Amazon basin as precipitation[12,13], which is further driven and maintained by forest cover[14,15]or reroutes air masses to the higher latitudes. The three Andean subregions (northern, central and southern) differ in their genesis[16] and the way in which they interact with atmospheric circulation, resulting in a wide range of environmental conditions. Uplift of the Northern Andes peaked in the late Neogene c. 12–4 Ma and is linked to the Neogene collision of the South American and Caribbean plates with the Panama Arch[17,18], which resulted in their characteristic trifurcate pattern. Neogene sedimentary records provide evidence of a change from high precipitation to arid conditions around 9 Ma, which is linked to the changing pattern of the South American low-level jet[8,19,20,21,22]. This process redefined landscape and biodiversity patterns in the Andes and Amazonia and shaped the basic geographic conditions of today[23]. A large portion of the Central Andes, in particular its extensive high-elevation Plateau (the Altiplano), uplifted rapidly and extensively during two distinct phases, between 30-25 Ma and, more notably, between 10-5 Ma[7]. The orographic history of the Southern Andes has been relatively less studied, but is summarised by refs [24,25,26], among others.

Vertebrate species richness is highest across the relatively young Northern Andes (Fig. 1). High species richness is strongly correlated with high annual rainfall, but temperature also plays an important role, as well as temperature range and precipitation seasonality (Figs. 3b, S6). Among geological variables, topographic relief and soil heterogeneity dominate (Figs. 3b, S6). In the relatively young northern Andes, high diversity may be related to surface uplift[27], which allowed the establishment and subsequent local diversification of cool-adapted lineages of animals[28] and plants[29,30], although a connection between diversification and orogeny is not always evident[31]. This area is also characterised by many recent species radiations, commonly linked to the influence of glacial-interglacial cycles[32,33,34,35]. In the older central Andes, the orographic barrier is particularly strong, with a warm, wet northeastern side supporting high diversity, and a colder and drier southwestern side with low diversity. In the southern Andes, precipitation patterns are opposite to those in the central and Northern Andes[11]. Predominant advection of moisture there comes from the Pacific and creates orographic rainfall in the west (where diversity is highest) and a prominent rain shadow, and fewer species of both plants and animals in Patagonia in the east.

Europe

High topographic heterogeneity characterises much of central Europe and adjacent Anatolia, as well as western Scandinavia. The major mountain belt—including the Alps, Carpathians, Pyrenees and associated ranges north of the Mediterranean Sea— resulted from orogenies in the late Mesozoic and middle to late Cenozoic[36] and run east-west, serving as orographic and dispersal barriers. Our regional analysis was performed on the Alps, Carpathians and Pyrenees.

Mountain vertebrate richness (Fig. 1) peaks in the Pyrenees, the western Alps, and the Balkans, and is lowest in Scandinavia. Central Europe is the only region where the absolute values of precipitation and temperature are not significant for predicting species richness, being replaced by the range of temperature and seasonality of precipitation (Figs. 3b, S7). A possible explanation for the differences with western North America, a region at similar latitude, includes the latitudinal (Europe) versus longitudinal (North America) topographic gradients and the differences in timing of the wet season between Europe and western North America. Europe also stands out as the only region where the number of soil types is a better predictor of mountain biodiversity than any other geological variable (Fig. 3b). This effect is positive and linear (Fig. S7). Erosion potential shows a negative effect, which may indicate the inhibiting effect of erosion on the carrying capacity of the landscape for species rich populations.

High Asia

The Central Asian Highlands (hereafter 'High Asia') extend over 4000 km and comprise the Qinghai-Tibetan Plateau and the Tianshan, Hindu-Kush, Himalayan and Hengduan Shan mountain regions. Climate in this region has been mainly driven by the interactions among mountain and plateau formation and atmospheric circulation patterns. The topographic history of High Asia has been intensely studied[37,38,39,40], key geological events being the Indo-Eurasian collision (ca. 55–40 Ma) and uplift of the Himalayas (ca. 20–15 Ma)[41,42]. Hengduan Shan might have a younger uplift history, mainly in the Pliocene[43]. Surface uplift events contributed to strengthen the Asian monsoon system (distinct wet/dry seasonality) in the Miocene[44,45], although a resilient system of monsoonal circulations existed at least since the Eocene. The onset of the monsoons was modulated by a combination of various factors, including Tibetan and Himalayan surface uplift, and possibly also the retreat of the Tarim Sea[46], changes in global atmospheric pCO$_2$[47] and global climate shifts including the Eocene-Oligocene transition[48] or general global cooling[49]. Further evidence for these events derive from fossil flora[50,51,52], windblown dust provenance, oxygen isotope-based palaeoclimate records, and climatic simulations[47,53,54]. The Qinghai-Tibetan Plateau forms a barrier to subtropical tropospheric airflow and pulls the Intertropical Convergence Zone seasonally far north of the equator[55], affecting the global distribution of heat and moisture[50,55], yet it seems to have limited influence on central Asian moisture transport through westerly winds[56].

High Asia harbours a high diversity of vertebrates (Fig. 1) as well as vascular plants[57]. Vertebrate diversity is highest in the southern and southeastern parts of the region, reflecting a strong positive effect of precipitation and temperature on species richness (Figs. 3b, S8). This region is under strong influence of both the South Asian and East Asian monsoons, which are captured in a similar way[50] as the humid atmospheric currents that reach the Northern and Central Andes. The environment is dominated by a warm, humid climate and subtropical-tropical vegetation[58], which co-occurs with high vertebrate diversity. In contrast, the temperature extremes on the plateau, which are reflected in high temperature seasonality,

coincide with low species diversity and explain the negative relationship between vertebrate diversity and temperature annual range (Fig. S8c). Among geological variables, erosion potential and soil types are the strongest predictors of vertebrate diversity (Fig. 3b). The highest erosion potential is found where climate and topographic gradients are strongest (Himalayan and Hengduan Shan mountain regions; Fig. S4), reflecting the strong interactions between climate and topography over different time scales. Biodiversity in this region stems from deep-time as well as recent speciation, accompanied by mountain uplift and related climate changes[59,60,61,,62, 63,64,65].

Australia

Australia as a low-lying continent has three key regions of elevated topography: the Carnarvon Range in the northwest, the Macdonnell ranges in the centre of the continent, and the Great Dividing Range, or Eastern Highlands, paralleling the eastern coast. Although Australian mountains are not high (the highest peak is Mt Kosciuszko at 2230 m), they range into alpine habitats, and at least in Queensland, have a marked impact on the local climate. Mountain precipitation exhibits large variation: the central and western mountains are very dry, compared to the mesic climate of the Great Dividing Range in the east. The southern portion of the Great Dividing Range was locally glaciated during the colder phases of the Pleistocene, and the region is still associated with periglacial environments and high lake stands[66] and has frosty winters. Highest vertebrate diversity in Australian mountains occurs in the Great Dividing Range.

The patterns of vertebrate species richness (Fig. 1) broadly mirror those of plants[67], with the highest species richness associated with the central portion of the Great Dividing Range near New England. Significant predictors of vertebrate diversity across Australian mountain ranges are temperature, precipitation and precipitation seasonality (Figs. 3b, S9). The negative correlation between vertebrate diversity and long-term erosion rate, not detected for any other mountain region, might reflect the Neogene uplift in the southern part of the Great Dividing Range, which may be associated with local aridification, and long term erosion flattening out the heterogeneity of the landscape, although the variation and scarcity in data points preclude definite conclusions.

B) Additional regions only included in the global analyses

Eastern South America

The mountains of eastern South America are generally older and lower than the Andes, ending their orogeny around 18–15 Ma[68] and reaching today less than half the elevation of the highest Andean mountains (ca. 2,900 m vs. ca. 7,000 m). There is a precipitation gradient from the coast to inland reflected by a transition in ecosystems, from the Atlantic rain forest with dense tropical vegetation on the eastern mountain slopes, replaced by open savanna vegetation (the Cerrado) on the Brazilian plateau (ca. 600–800 m), and shrublands in the

semi-arid Caatinga of northeastern Brazil. The Caatinga, Cerrado, Chaco and Pantanal form together a diagonal belt of seasonally dry vegetation that act as a biogeographical barrier for mountain and rain forest organisms. Vertebrate diversity has not only been linked to current climate but also to the effect of vegetation stability, in particular refugia, through Quaternary climatic cycles[69]. Mountain vertebrate diversity peaks in southeastern Brazil, following a reverse latitudinal diversity gradient previously reported for birds[70].

Eastern Africa

The geological and climatic history of eastern Africa is in stark contrast to that in southern Africa. In eastern Africa, much of the topography and mountain building reflects the development of the East African Rift system (Western and Eastern Rift) during the Miocene[71]. The mountains in this region are consequently much younger than the southern African mountains, and major mountain ranges, such as the Rwenzori, date only from the Pliocene[72].

Southern Africa

Southern Africa is dominated by a central plateau (1000–2000 m), with the highest peaks reaching 3000 m. The plateau is separated by an abrupt escarpment from a narrow coastal plain, which both have been in place throughout the Cenozoic and probably since the continental breakup in the Jurassic[73]. At the break-up of Pangea in the late Jurassic, the escarpment was on the continental margins, and rapid erosion during the Cretaceous resulted in the retreat of the escarpment to its present position, with apparently little further retreat during the Cenozoic[74]. During this process, the Cape Fold Mountains were exhumed. These are composed of a resistant quartzitic sandstone, and have probably retained their steep slopes and craggy peaks throughout the Cenozoic[75]. The eastern half of the subcontinent, centred around the Drakensberg, was however uplifted by up to 900 m during the Pliocene, increasing its topography[73]. The eastern escarpment and coastal plain are today much wetter than the western escarpment and coastal plain, and an east-west aridity gradient extends across the central plateau[76]. The gradual aridification of the western half of the subcontinent since the middle Miocene[77,78] has led to the establishment of a summer-dry and winter-wet climate at the southwestern tip of the continent[79]. The huge plant diversity of southern Africa[80], especially the Cape flora which contains an extreme level of endemism, has been linked to this Mediterranean-type climate, topographic barriers (resistant sandstones), and long-term geological and climatic stability[81,82]. The low vertebrate diversity in the southwestern part of the subcontinent, from southern Namibia to Port Elizabeth (the winter-rainfall region), could be caused by the dominant sclerophyllous vegetation.

II. Supplementary tables and figures

Supplementary Table S1: **Predictor variables** used for analysing vertebrate species richness across the world's mountains and their main biological importance.

Abbreviation	Description	Unit	Source [resolution]	Biological importance
PREC	Annual precipitation	mm yr^{-1}	CHELSA (version 1.2)[83] [30 arc sec]	Sustaining vegetation and associated biota
TEMP	Mean annual temperature	°C × 10	CHELSA (version 1.2)[83] [30 arc sec]	Influences biomass productivity and reflects energy availability
TEMP RANGE	Temperature annual range (maximum temperature of warmest month minus minimum temperature of coldest month)	°C × 10	CHELSA (version 1.2)[83] [30 arc sec]	Selective filter for species, e.g. frost tolerance. Drives physiological adaptations and behavioural strategies
PREC SEASON	Precipitation seasonality (coefficient of variation of monthly values)	mm	CHELSA (version 1.2)[83] [30 arc sec]	Selective filter for species, e.g. drought tolerance. Drives physiological adaptations and life cycle strategies
RELIEF	Topographic relief measured as mean of elevation range values (max-min) within 2.5 km radii for each 90 m resolution pixel	m	Calculated using EarthEnv-DEM90 [84] [90 m]	Determines microclimate and fine-scale biotic composition across elevational zones affecting alpha and beta diversity
LONG EROSION	Long-term erosion calculated using low temperature thermochronology (fission-track and (U-Th)/He for apatite and zircon)	km Myr^{-1}	Calculated using the dataset by ref. [85].	Interacts with rock uplift in regulating the dynamics of landscape changes and new opportunities (habitats, ecological niches) for speciation
EROSION POTENTIAL	Unit stream power (USP) index weighted with precipitation data, i.e. rate of energy loss to channel bed per unit length (energy per unit time), calculated as $$USP = \sum (A_s P)^{1/2} S$$ where A_P is upstream drainage area (used as a proxy of discharge) for each pixel, P is the average precipitation from 1998–2007 and S is local slope. The formula sums the flow-lines to calculate the flow accumulation	Wm^{-1}	Calculated using the SRTM 90 m database v.4.1[86]. Precipitation data for period 1998–2007[87,88]	Influences vegetation dynamics, e.g. through ecological successions in connection with landslides. Also related to critical zone properties (soil thickness, soil properties, and soil and rock weathering state), which in turn filter the taxonomic composition of the aboveground vegetation and associated fauna
SOIL	Number of soil types	count	SoilGrids1km[89] [1 km]	Influences habitat heterogeneity, filtering for vegetation types and associated biotas

Supplementary Table S2: **Characteristics of the global mountain dataset** in relation to variation in vertebrate species richness, climate, and geology. The dataset covered a total of 585 grid cells with global extent (Fig. 3a in main text) and a spatial resolution of 1º × 1º. For abbreviation and units of predictor variables see Table S1.

Variable	Minimum	Median	Mean	Maximum
Vertebrate species richness	25	241	290	1135
PREC	0.20	926	1098	5921
TEMP	-88	103	112	175
TEMP RANGE	47	227	223	504
PREC SEASON	5	48	56	332
RELIEF	60	902	1387	5076
LONG EROSION	0.01	0.13	0.16	0.94
EROSION POT	0.19	46	104	1586
SOIL	2	12	12	22

Supplementary Table S3: **Results from global multi-predictor regression models** to explain vertebrate species richness across the world's mountains ($n = 585$ grid cells with a spatial resolution of 1º × 1º). Two types of models are compared, a non-spatial ordinary least square (OLS) regression and a spatial simultaneous autoregressive (SAR) model. The response variable (vertebrate species richness) as well as long-term erosion, current erosion potential and relief variables were log-transformed. Using the full OLS multi-predictor model (i.e. including all eight predictor variables), a model selection was performed with the Akaike Information Criterion (AIC) to derive a minimum adequate model. All variables were scaled to a mean of zero and variance of 1 before the analysis to make model coefficients comparable. Predictor variables that were removed by AIC model selection are indicated with '−'. Standardised coefficients, the explained variance of the environmental components (R^2_{PRED}), the explained variance of the full SAR model including both environment and space (R^2_{FULL}), the Moran's I, and the p-value of Moran's I are given. Significance of Moran's I was determined by permutation tests ($n = 999$ permutations). Significance levels: ***$p < 0.001$; **$p < 0.01$; *$p < 0.05$. n.s., not significant. Abbreviations and explanations of predictor variables are found in Table 1 and Table S1.

	OLS		SAR	
	Coefficient	p	Coefficient	p
Intercept	5.461	***	5.451	***
PREC	0.330	***	0.245	***
TEMP	0.390	***	0.169	***
TEMP RANGE	0.102	***	0.003	n.s.
PREC SEASON	−		−	
RELIEF	0.429	***	0.146	***
LONG EROSION	-0.083	***	0.014	n.s.
EROSION POT	−		−	
SOIL	0.158	***	0.081	***
R^2_{PRED}	0.54		0.43	
R^2_{FULL}	−		0.92	
Moran's I	0.760	***	-0.015	n.s.

Supplementary Table S4: Results from regional multi-predictor regression models to explain vertebrate species richness in the mountains of western North America, the Andes, central Europe, High Asia, and eastern Australia. Two types of models are compared, a non-spatial ordinary least square (OLS) regression and a spatial simultaneous autoregressive (SAR) model. Using the full OLS multi-predictor model (i.e. including all eight predictor variables), a model selection was performed with the Akaike Information Criterion (AIC) to derive a minimum adequate model. The response variable (vertebrate species richness) as well as long-term erosion, current erosion potential and relief variables were log-transformed. All variables were scaled to a mean of zero and variance of 1 before the analysis to make model coefficients comparable. Predictor variables that were removed by AIC model selection are indicated with '–'. Standardised coefficients, the explained variance of the environmental components (R^2_{PRED}), the explained variance of the full SAR model including both environment and space (R^2_{FULL}), the Moran's I, and the p-value of Moran's I are given. Significance of Moran's I was determined by permutation tests ($n = 999$ permutations). Significance levels: ***$p < 0.001$; **$p < 0.01$; *$p < 0.05$. n.s., not significant. Abbreviations and explanations of predictor variables are found in Table 1 and Table S1.

|	North America		The Andes		Central Europe	
	OLS	SAR	OLS	SAR	OLS	SAR
Intercept	0 n.s.	-0.058 n.s.	0 n.s.	0.015 n.s.	0 n.s.	-0.024 n.s.
PREC	0.377***	0.187 n.s.	0.717***	0.669***	–	–
TEMP	0.959***	0.651***	0.546***	0.499***	–	–
TEMP RANGE	–		-0.188***	-0.244***	0.819***	0.889***
PREC SEASON	–		0.121 n.s.	0.165*	-0.361***	-0.133 n.s.
RELIEF	0.910***	0.646***	0.561***	0.501***	–	–
LONG EROSION	–	–	–	–	–	–
EROSION POT	–	–	–	–	-0.154 n.s.	-0.125 n.s.
SOIL	0.333***	0.258***	0.083 n.s.	0.111**	0.262**	0.106 n.s.
R^2_{PRED}	0.73	0.72	0.91	0.90	0.70	
R^2_{FULL}	–	0.82	–	0.93	–	
Moran's I	0.295***	-0.032 n.s.	0.326***	-0.012 n.s.	0.233**	

|	High Asia		Australia	
	OLS	SAR	OLS	SAR
Intercept	0 [n.s.]	-0.078 [n.s.]	0 [n.s.]	0.087 [n.s.]
PREC	0.312***	0.201**	0.973***	-0.164 [n.s.]
TEMP	0.213**	0.095*	1.092***	-0.114 [n.s.]
TEMP RANGE	-0.363***	-0.372***	–	–
PREC SEASON	-0.091 [n.s.]	-0.096 [n.s.]	-0.366*	0.111 [n.s.]
RELIEF	–	–	0.425*	-0.062 [n.s.]
LONG EROSION	–	–	-0.290*	-0.016 [n.s.]
EROSION POT	0.202***	0.021 [n.s.]	–	–
SOIL	0.111*	0.050 [n.s.]	0.349 [n.s.]	0.013 [n.s.]
R^2_{PRED}	0.79	0.76	0.59	0.19
R^2_{FULL}	–	0.94	–	0.93
Moran's I	0.495***	0.030 [n.s.]	0.297**	-0.025 [n.s.]

Supplementary Table S5: Correlation matrix showing Spearman rank correlations between species richness (SR) and all eight predictor variables (see Table S1 for abbreviations).

| Variable	SR	TEMP	TEMP RANGE	PREC	PREC SEASON	RELIEF	LONG EROSION	EROSION POT	SOIL
SR	1	0.37	-0.16	0.30	0.16	0.19	0.06	0.25	0.17
TEMP		1	-0.49	0.22	0.12	-0.42	-0.24	-0.25	-0.01
TEMP RANGE			1	-0.59	0.16	0.39	0.05	0.04	-0.29
PREC				1	-0.35	-0.38	0.13	0.16	0.37
PREC SEASON					1	0.49	0.03	0.13	-0.33
RELIEF						1	0.38	0.48	-0.30
LONG EROSION							1	0.50	-0.02
EROSION POT								1	0.09
SOIL									1
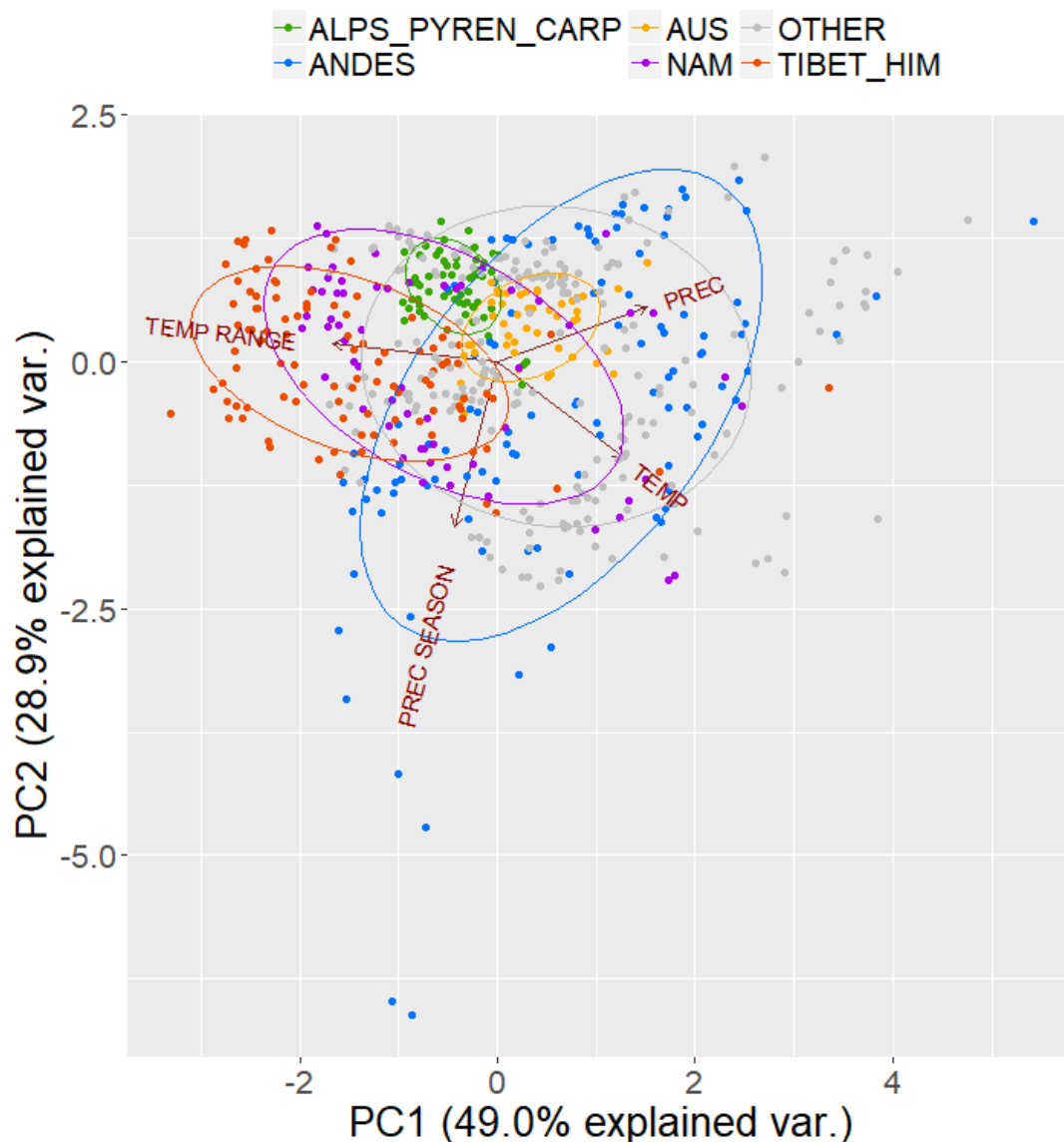
Supplementary Figure S1 | Climate space and the location of mountain regions. For the global dataset covering 585 grid cells at 1° resolution, a Principal Component Analysis (PCA) was run with the four climatic predictor variables (PREC, TEMP, TEMP RANGE and PREC SEASON, see Table S3). The first two axes (PC1 and PC2) were retained (explaining together 78% of climate variation) and the five mountain regions of the regional analyses were plotted within this climate space. Coloring corresponds to the regions in Fig. 3. ALPS_PYREN_CARP = central Europe including the European Alps, Pyrenees and Carpathians; ANDES = the Andes including the northern, central and southern subregions; AUS = Australia including the Carnarvon Range, Macdonnell ranges and the Great Dividing Range; NAM = western North America including the North American Cordillera; TIBET_HIM = High Asia including the Qinghai-Tibetan Plateau, Tianshan, Hindu-Kush, Himalayan and Hengduan Shan mountains; OTHER = all other mountain regions not analyzed separately (due to low regional sample sizes).
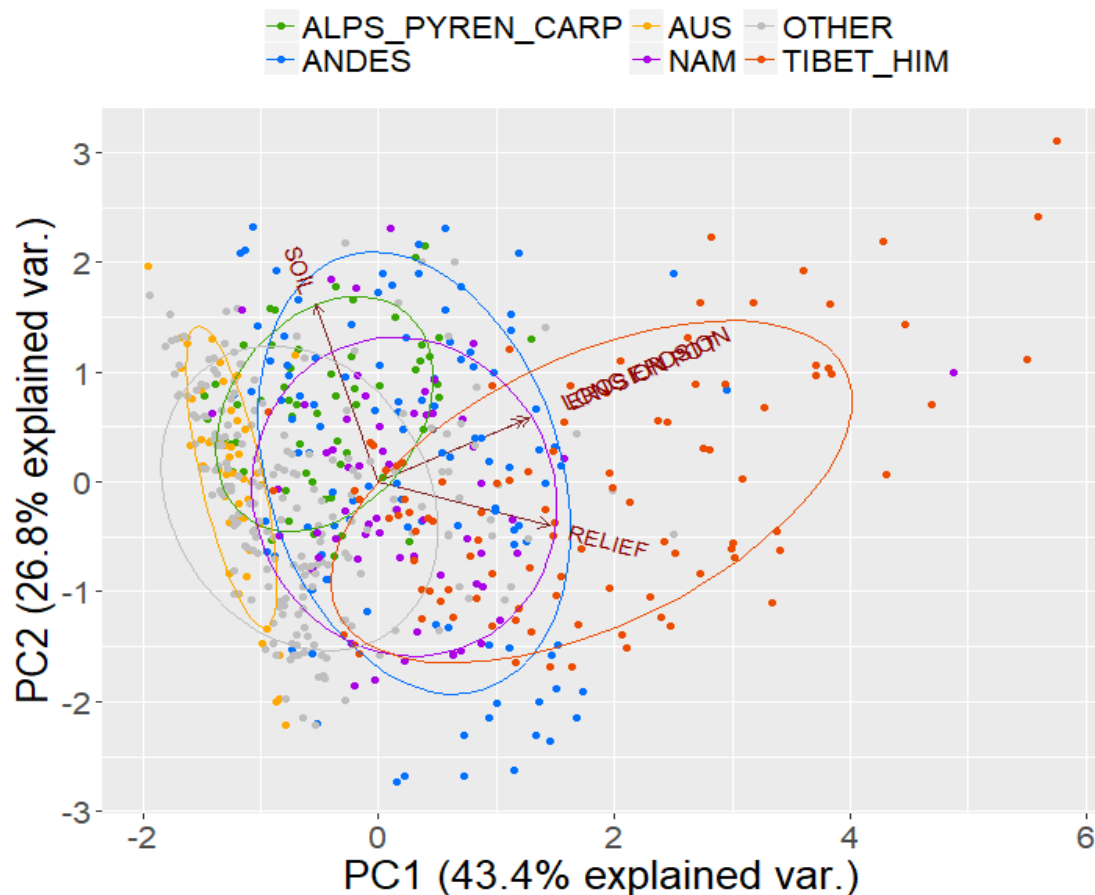
Supplementary Figure S2 | Geological space and the location of mountain regions. For the global dataset covering 585 grid cells at 1° resolution, a Principal Component Analysis (PCA) was run with the four geological predictor variables (LONG EROSION and EROSION POT, which are fully overlain, and RELIEF and SOIL; see Table S3). The first two axes (PC1 and PC2) were retained (explaining together 70% of geological variation) and the five mountain regions of the regional analyses were plotted within this geological space. Coloring corresponds to the regions in Figure 3. ALPS_PYREN_CARP = central Europe including the European Alps, Pyrenees and Carpathians; ANDES = the Andes including the northern, central and southern subregions; AUS = Australia including the Carnarvon Range, Macdonnell ranges and the Great Dividing Range; NAM = western North America including the North American Cordillera; TIBET_HIM = High Asia including the Qinghai-Tibetan Plateau, Tianshan, Hindu-Kush, Himalayan and Hengduan Shan mountains; OTHER = all other mountain regions not analyzed separately (due to low regional sample sizes).
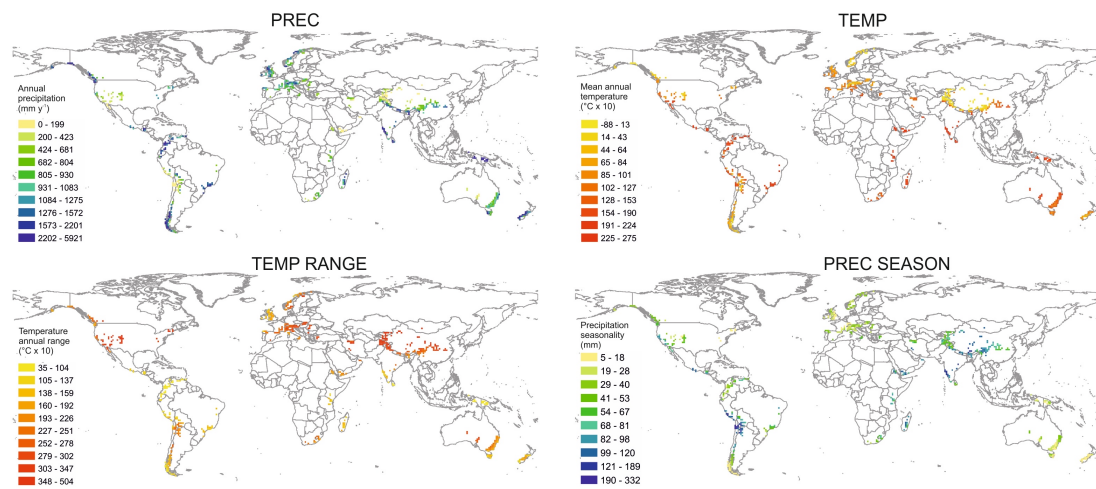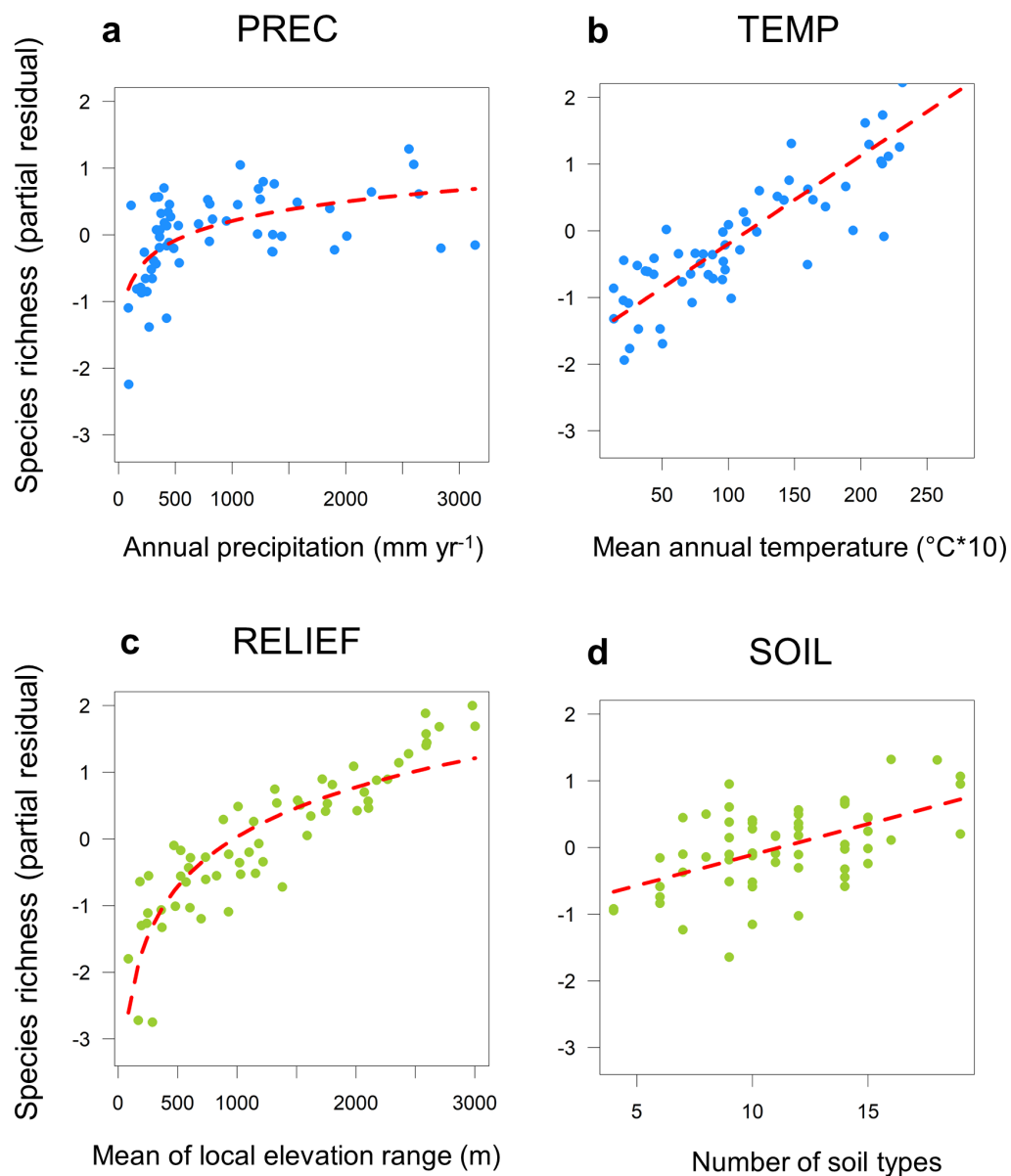
Supplementary Figure S3 | Climatic predictor variables and their global variation across all included 1º grid cells (*n* = 585). Maps are plotted with quantile classification and a World Geodetic System projection (WGS 1984). See Table S1 for details on predictor variables.
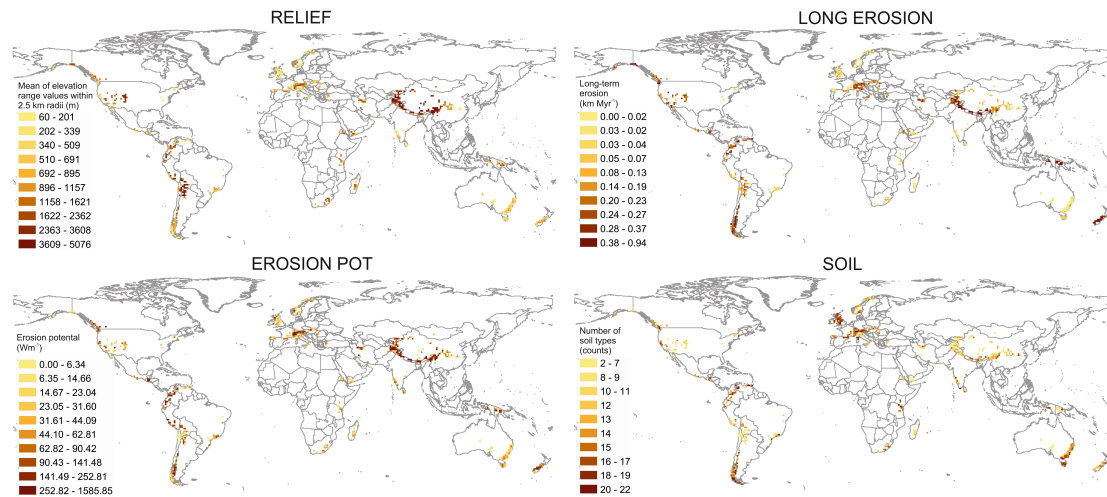
Supplementary Figure S4. Geological predictor variables and their global variation across all included 1º grid cells (*n* = 585). Maps are plotted with quantile classification and a World Geodetic System projection (WGS 1984). See Table S1 for details on predictor variables.
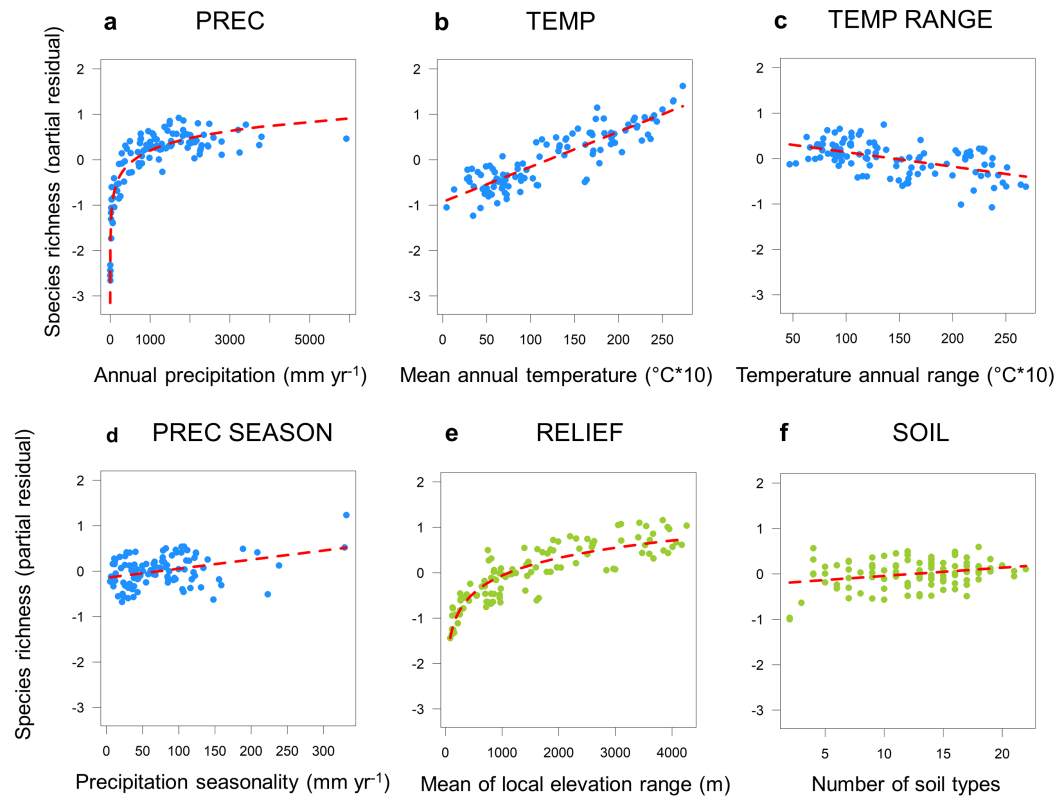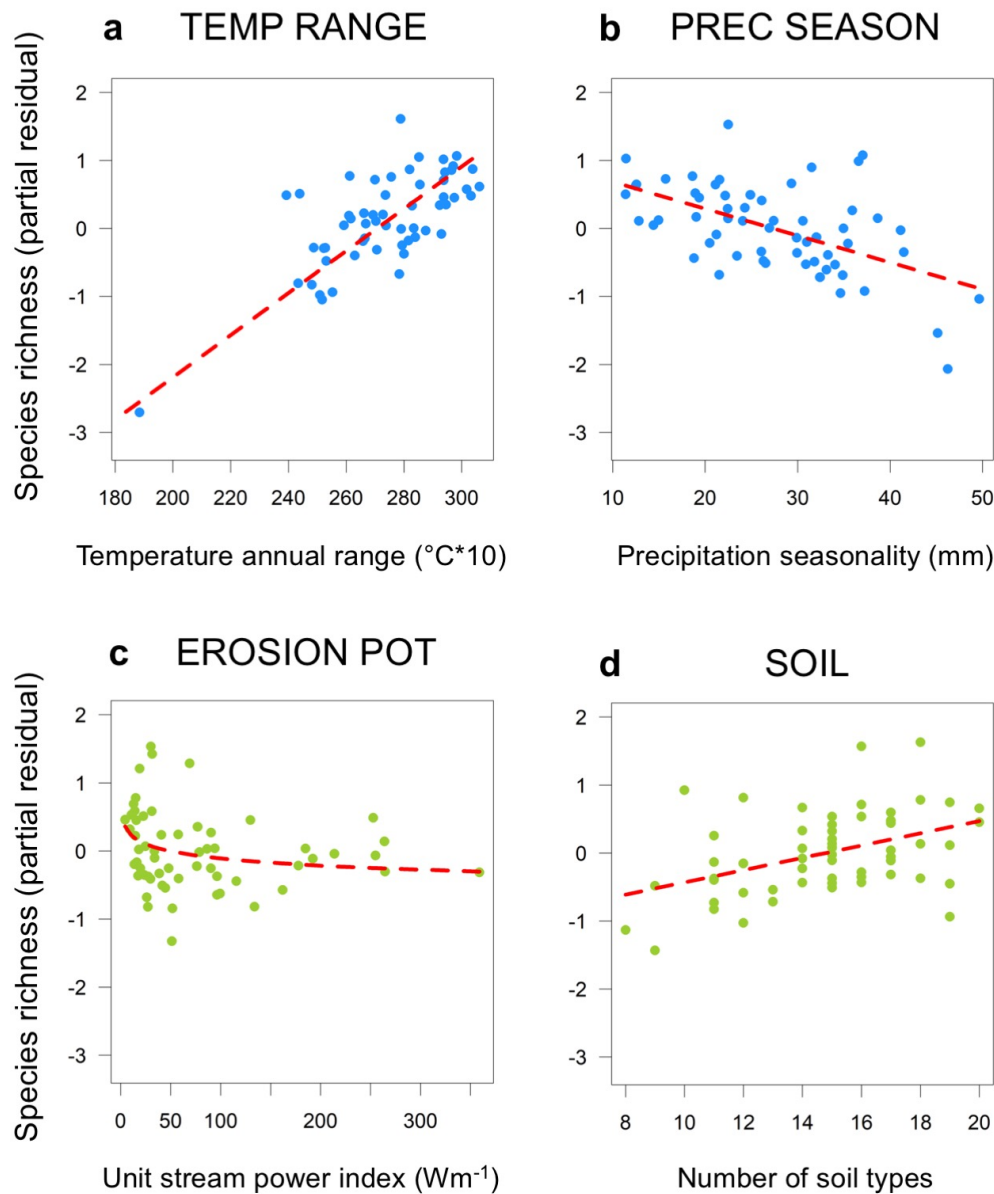
North America

Supplementary Figure S5 | Determinants of vertebrate species richness for western North America. Partial residual plots of predictor variables (**a–d**) from regional multi-predictor model across 1° grid cells (see Table S4), relating species richness of vertebrates to climatic (blue) and geological (green) predictor variables. Partial residuals represent the relationship between a response and a predictor variable when all other predictor variables in the model are statistically controlled. Predictor variables are explained in Table S1.
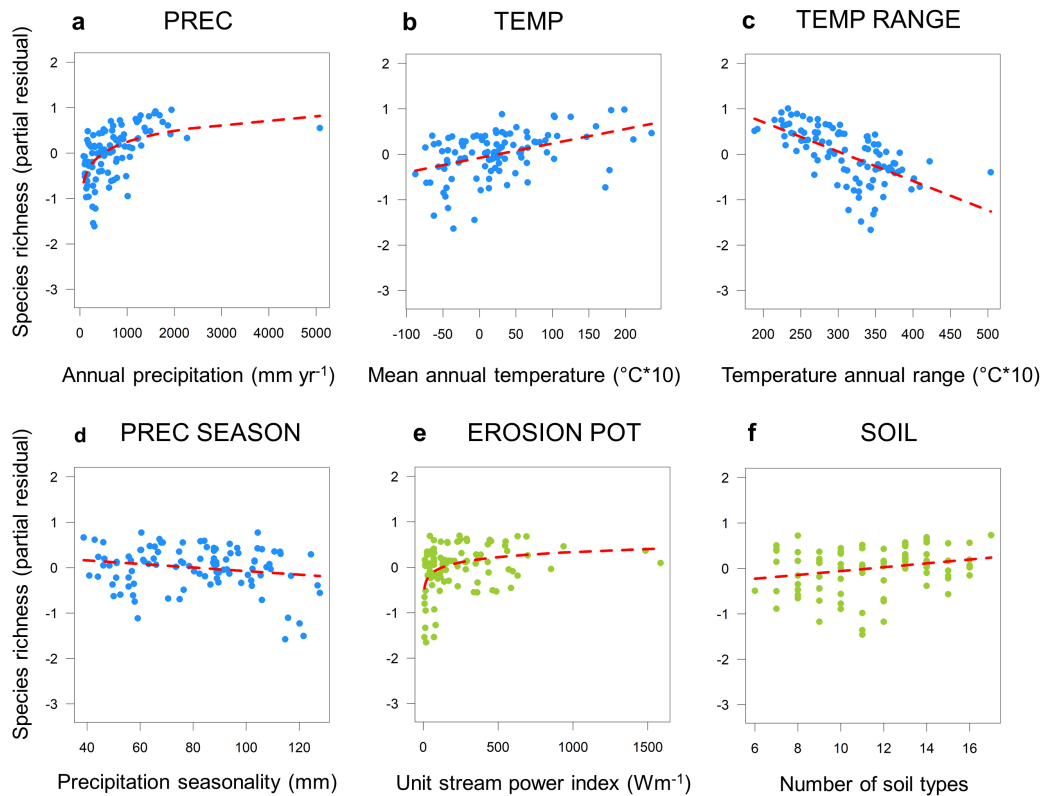
Supplementary Figure S6 | Determinants of vertebrate species richness for the Andes. Partial residual plots of predictor variables (**a–f**) from regional multi-predictor model across 1° grid cells (see Table S4), relating species richness of vertebrates to climatic (blue) and geological (green) predictor variables. Partial residuals represent the relationship between a response and a predictor variable when all other predictor variables in the model are statistically controlled. Predictor variables are explained in Table S1.

Central Europe

Supplementary Figure S7 | Determinants of vertebrate species richness for central Europe. Partial residual plots of predictor variables (**a–d**) from regional multi-predictor model across 1° grid cells (see Table S4), relating species richness of vertebrates to climatic (blue) and geological (green) predictor variables. Partial residuals represent the relationship between a response and a predictor variable when all other predictor variables in the model are statistically controlled. Predictor variables are explained in Table S1.

High Asia

Supplementary Figure S8 | Determinants of vertebrate species richness for High Asia. Partial residual plots of predictor variables (**a–f**) from regional multi-predictor model across 1° grid cells (see Table S4), relating species richness of vertebrates to climatic (blue) and geological (green) predictor variables. Partial residuals represent the relationship between a response and a predictor variable when all other predictor variables in the model are statistically controlled. Predictor variables are explained in Table S1.
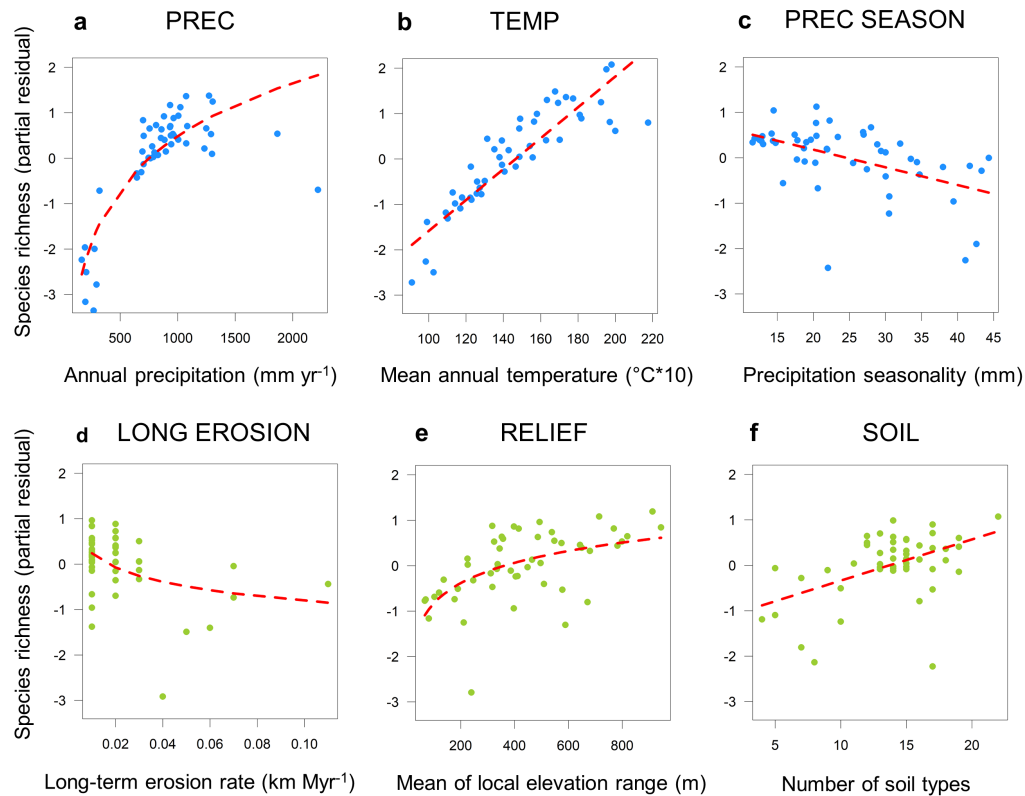
Australia

Supplementary Figure S9 | Determinants of vertebrate species richness for Australia. Partial residual plots of predictor variables (**a–f**) from regional multi-predictor model across 1° grid cells (see Table S4), relating species richness of vertebrates to climatic (blue) and geological (green) predictor variables. Partial residuals represent the relationship between a response and a predictor variable when all other predictor variables in the model are statistically controlled. Predictor variables are explained in Table S1.
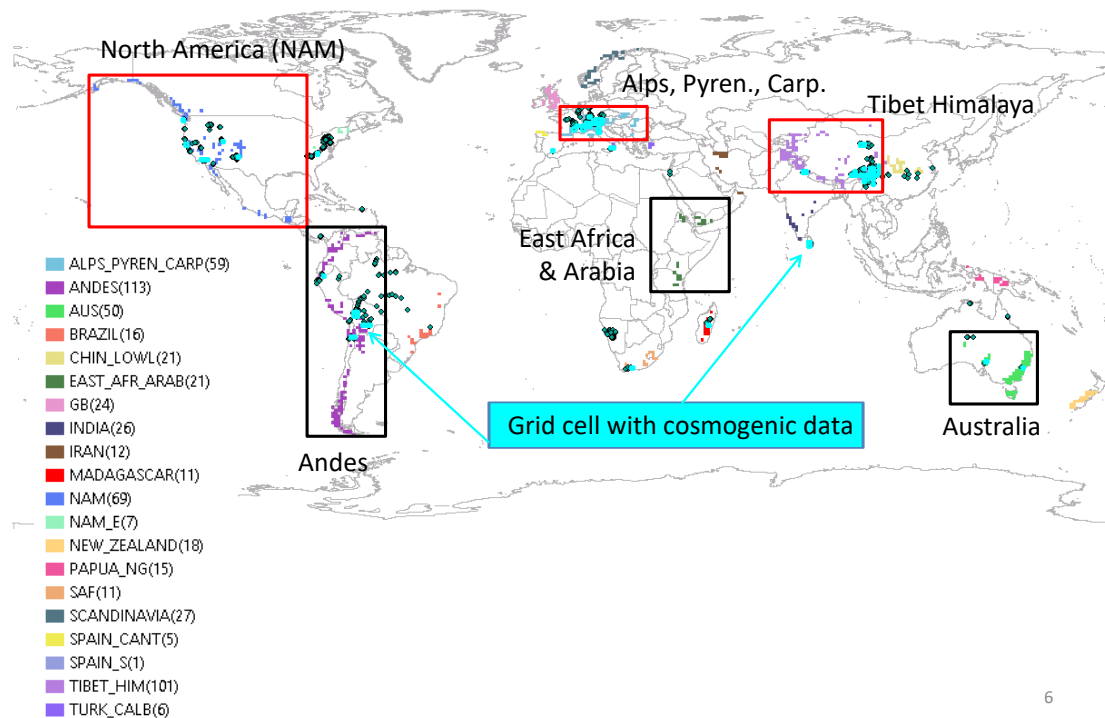
Supplementary Figure S10 | Data compilation from different mountain ranges around the world. The figure shows the number of grid cells for which we were able to obtain all geological, climatic and biological variables included in this study. See colour legend for each mountain range or region. The blue dots represent those cells for which cosmogenic isotope-derived millennial-scale erosion data ref. [90] were also available. Although this erosion variable would have been suitable for our analyses, the relatively small overlap with the rest of our dataset led us to calculate alternative erosion metrics.
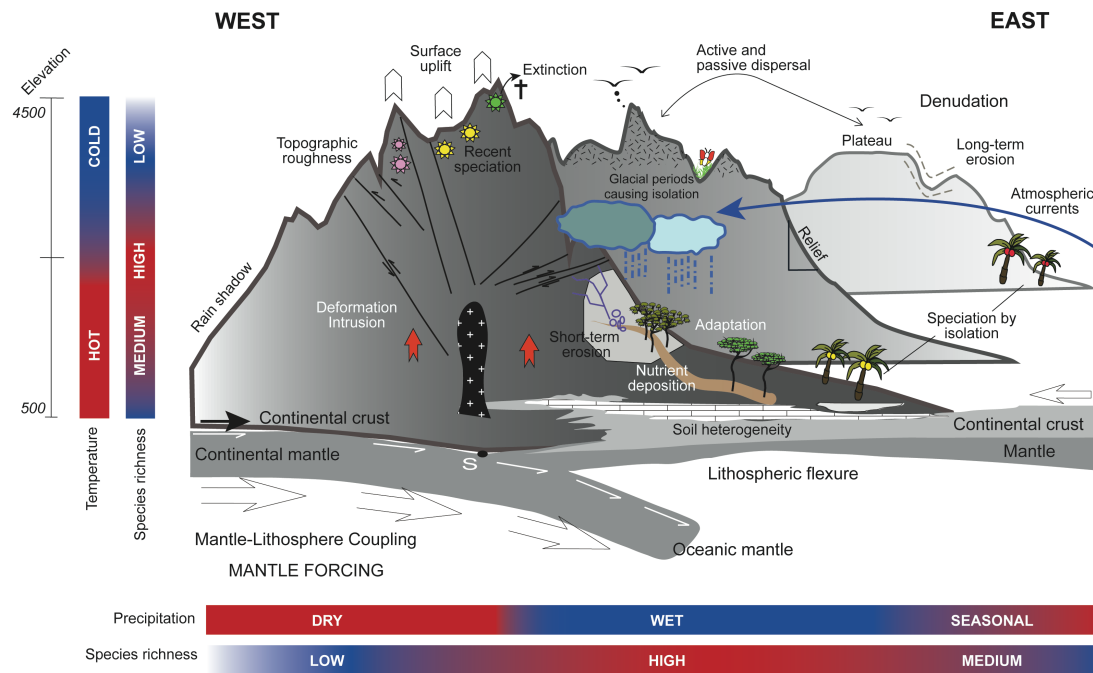
Supplementary Figure S11 | Hypothetical west-to-east cross section of a mountain range with an indication of where climatic, geological and biological processes take place in mountains. As mountains develop, lowland organisms may become isolated and speciate due to the lack of genetic interchange. Some species colonise new mountains through long-distance dispersal and local recruitment from lowlands. Plants and the ecosystems they define adapt to different soil types and nutrient levels. Surface uplift leads to the formation of new habitats that trigger rapid speciation and the accumulation of local endemics. High-elevation species that cannot adapt to warmer climates either move elsewhere or go extinct; others are relicts from glacial periods. High species richness generally coincides with warm and humid conditions, in regions of high relief and soil heterogeneity and low levels of erosion.

III. Supplementary References

1.   Dickinson, W. R. Evolution of the North American Cordillera. *Annual Review of Earth and Planetary Sciences* **32,** 13–45 (2004).

2.   Champagnac, J.-D., Molnar, P., Sue, C. & Herman, F. Tectonics, climate, and mountain topography. *J. Geophys. Res.* **117,** B02403 (2012).

3.   Keith, H., Mackey, B. G. & Lindenmayer, D. B. Re-evaluation of forest biomass carbon stocks and lessons from the world's most carbon-dense forests. *PNAS* **106,** 11635–11640 (2009).

4.   Badgley, C. & Fox, D. L. Ecological biogeography of North American mammals: species density and ecological structure in relation to environmental gradients. *Journal of Biogeography* **27,** 1437–1467 (2000).

5.   Currie, D. J. Energy and Large-Scale Patterns of Animal- and Plant-Species Richness. *The American Naturalist* **137,** 27–49 (1991).

6.   Kent-Corson, M. L., Barnosky, A. D., Mulch, A., Carrasco, M. A. & Chamberlain, C. P. Possible regional tectonic controls on mammalian evolution in western North America. *Palaeogeography, Palaeoclimatology, Palaeoecology* **387,** 17–26 (2013).

7.   Garzione, C. N. *et al.* Rise of the Andes. *Science* **320,** 1304–1307 (2008).

8.   Mulch, A., Uba, C. E., Strecker, M. R., Schoenberg, R. & Chamberlain, C. P. Late Miocene climate variability and surface elevation in the central Andes. *Earth and Planetary Science Letters* **290,** 173–182 (2010).

9.   Poulsen, C. J., Ehlers, T. A. & Insel, N. Onset of Convective Rainfall During Gradual Late Miocene Rise of the Central Andes. *Science* **328,** 490–493 (2010).

10. Sepulchre, P., Sloan, L. C. & Fluteau, F. Modelling the Response of Amazonian Climate to the Uplift of the Andean Mountain Range. in *Amazonia: Landscape and Species Evolution* (eds. Hoorn, C. & Wesselingh, F. P.) 211–222 (Wiley-Blackwell Publishing Ltd., 2010).

11. Flantua, S. G. A. *et al.* Climate variability and human impact in South America during the last 2000 years: synthesis and perspectives from pollen records. *Climate of the Past* **12,** 483–523 (2016).

12. Garreaud, R. D., Vuille, M., Compagnucci, R. & Marengo, J. Present-day South American climate. *Palaeogeography, Palaeoclimatology, Palaeoecology* **281,** 180–195 (2009).

13. Barnes, J. B., Ehlers, T. A., Insel, N., McQuarrie, N. & Poulsen, C. J. Linking orography, climate, and exhumation across the central Andes. *Geology* **40,** 1135–1138 (2012).

14. Makarieva, A. M. & Gorshkov, V. G. Biotic pump of atmospheric moisture as driver of the hydrological cycle on land. *Hydrol. Earth Syst. Sci.* **11,** 1013–1033 (2007).

15. Wright, J. S. *et al.* Rainforest-initiated wet season onset over the southern Amazon. *Proceedings of the National Academy of Sciences* 201621516 (2017). doi:10.1073/pnas.1621516114

16. Elsen, P. R. & Tingley, M. W. Global mountain topography and the fate of montane species under climate change. *Nature Clim. Change* **5,** 772–776 (2015).

17. Boschman, L. M., van Hinsbergen, D. J. J., Torsvik, T. H., Spakman, W. & Pindell, J. L. Kinematic reconstruction of the Caribbean region since the Early Jurassic. *Earth-Science Reviews* **138,** 102–136 (2014).

18. Bermúdez, M. A. *et al.* The detrital record of late-Miocene to Pliocene surface uplift and exhumation of the Venezuelan Andes in the Maracaibo and Barinas foreland basins. *Basin Res* **29,** 370–395 (2017).

19. Strecker, M. R. *et al.* Tectonics and Climate of the Southern Central Andes. *Annual Review of Earth and Planetary Sciences* **35,** 747–787 (2007).

20. Rohrmann, A. *et al.* Can stable isotopes ride out the storms? The role of convection for water isotopes in models, records, and paleoaltimetry studies in the central Andes. *Earth and Planetary Science Letters* **407,** 187–195 (2014).

21. Rohrmann, A. *et al.* Miocene orographic uplift forces rapid hydrological change in the southern central Andes. *Scientific Reports* **6,** 35678 (2016).

22. Pingel, H. *et al.* Pliocene orographic barrier uplift in the southern Central Andes. *Geology* **42,** 691–694 (2014).

23. Hoorn, C. *et al.* Amazonia Through Time: Andean Uplift, Climate Change, Landscape Evolution, and Biodiversity. *Science* **330,** 927–931 (2010).

24. Ramos, V. A. Plate tectonic setting of the Andean Cordillera. *Episodes* **22,** 183–190 (1999).

25. Viale, M. & Garreaud, R. Orographic effects of the subtropical and extratropical Andes on upwind precipitating clouds. *Journal of Geophysical Research: Atmospheres* **120,** 4962–4974 (2015).

26. Horton, B. K. Tectonic Regimes of the Central and Southern Andes: Responses to Variations in Plate Coupling During Subduction. *Tectonics* **37,** 402–429 (2018).

27. Luebert, F. & Weigend, M. Phylogenetic insights into Andean plant diversification. *Front. Ecol. Evol* **2,** 1–17 (2014).

28. Fjeldså, J., Bowie, R. C. K. & Rahbek, C. The Role of Mountain Ranges in the Diversification of Birds. *Annual Review of Ecology, Evolution, and Systematics* **43,** 249–265 (2012).

29. Antonelli, A., Nylander, J. A. A., Persson, C. & Sanmartín, I. Tracing the impact of the Andean uplift on Neotropical plant evolution. *PNAS* **106,** 9749–9754 (2009).

30. Sanín, M. J. *et al.* The Neogene rise of the tropical Andes facilitated diversification of wax palms (Ceroxylon: Arecaceae) through geographical colonization and climatic niche separation. *Botanical Journal of the Linnean Society* **182,** 303–317 (2015).

31. Mutke, J., Jacobs, R., Meyers, K., Henning, T. & Weigend, M. Diversity patterns of selected Andean plant groups correspond to topography and habitat dynamics, not orogeny. *Frontiers in Genetics* **5,** (2014).

32. Hughes, C. & Eastwood, R. Island radiation on a continental scale: Exceptional rates of plant diversification after uplift of the Andes. *PNAS* **103,** 10334–10339 (2006).

33. Diazgranados, M. & Barber, J. C. Geography shapes the phylogeny of frailejones (Espeletiinae Cuatrec., Asteraceae): a remarkable example of recent rapid radiation in sky islands. *PeerJ* **5,** e2968 (2017).

34. Nevado, B., Contreras-Ortiz, N., Hughes, C. & Filatov, D. A. Pleistocene glacial cycles drive isolation, gene flow and speciation in the high elevation Andes. *New Phytologist* 219, 779-793 (2018).

35. Flantua, S. G. A. & Hooghiemstra, H. Historical connectivity and mountain biodiversity. in *Mountains, climate and biodiversity* (eds. Hoorn, C., Perrigo, A. & Antonelli, A.) 171–185 (Wiley-Blackwell, 2018).

36. Schmid, S. M., Fügenschuh, B., Kissling, E. & Schuster, R. Tectonic map and overall architecture of the Alpine orogen. *Eclogae geol. Helv.* **97,** 93–117 (2004).

37. Mulch, A. & Chamberlain, C. P. Earth science: The rise and growth of Tibet. *Nature* **439,** 670–671 (2006).

38. Rowley, D. B. & Currie, B. S. Palaeo-altimetry of the late Eocene to Miocene Lunpola basin, central Tibet. *Nature* **439,** 677–681 (2006).

39. Saylor, J. E. *et al.* The late Miocene through present paleoelevation history of southwestern Tibet. *Am J Sci* **309,** 1–42 (2009).

40. Ding, L. *et al.* The Andean-type Gangdese Mountains: Paleoelevation record from the Paleocene–Eocene Linzhou Basin. *Earth and Planetary Science Letters* **392,** 250–264 (2014).

41. Yin, A. & Harrison, T. M. Geologic Evolution of the Himalayan-Tibetan Orogen. *Annual Review of Earth and Planetary Sciences* **28,** 211–280 (2000).

42. Gébelin, A. *et al.* The Miocene elevation of Mount Everest. *Geology* G34331.1 (2013). doi:10.1130/G34331.1

43. Sun, B.-N. *et al.* Reconstructing Neogene vegetation and climates to infer tectonic uplift in western Yunnan, China. *Palaeogeography, Palaeoclimatology, Palaeoecology* **304,** 328–336 (2011).

44. Sun, X. & Wang, P. How old is the Asian monsoon system?—Palaeobotanical records from China. *Palaeogeography, Palaeoclimatology, Palaeoecology* **222,** 181–222 (2005).

45. Guo, Z. T. *et al.* A major reorganization of Asian climate by the early Miocene. *Clim. Past* **4,** 153–174 (2008).

46. Bosboom, R. *et al.* Linking Tarim Basin sea retreat (west China) and Asian aridification in the late Eocene. *Basin Res* **26,** 621–640 (2014).

47. Licht, A. *et al.* Asian monsoons in a late Eocene greenhouse world. *Nature* **513,** 501–506 (2014).

48. Dupont-Nivet, G. *et al.* Tibetan plateau aridification linked to global cooling at the Eocene–Oligocene transition. *Nature* **445,** 635–638 (2007).

49. Jiang, H. & Ding, Z. A 20 Ma pollen record of East-Asian summer monsoon evolution from Guyuan, Ningxia, China. *Palaeogeography, Palaeoclimatology, Palaeoecology* **265,** 30–38 (2008).

50. Molnar, P., Boos, W. R. & Battisti, D. S. Orographic Controls on Climate and Paleoclimate of Asia: Thermal and Mechanical Roles for the Tibetan Plateau. *Annual Review of Earth and Planetary Sciences* **38,** 77–102 (2010).

51. Quan, C., Liu, Y.-S. (C.) & Utescher, T. Eocene monsoon prevalence over China: A paleobotanical perspective. *Palaeogeography, Palaeoclimatology, Palaeoecology* **365–366,** 302–311 (2012).

52. Shukla, A., Mehrotra, R. C., Spicer, R. A., Spicer, T. E. V. & Kumar, M. Cool equatorial terrestrial temperatures and the South Asian monsoon in the Early Eocene:

Evidence from the Gurha Mine, Rajasthan, India. *Palaeogeography, Palaeoclimatology, Palaeoecology* **412,** 187–198 (2014).

53. Huber, M. & Goldner, A. Eocene monsoons. *Journal of Asian Earth Sciences* **44,** 3–23 (2012).

54. Licht, A. *et al.* Resilience of the Asian atmospheric circulation shown by Paleogene dust provenance. *Nature Communications* **7,** 12390 (2016).

55. Lippert, P. C., Hinsbergen, D. J. J. van & Dupont-Nivet, G. Early Cretaceous to present latitude of the central proto-Tibetan Plateau: A paleomagnetic synthesis with implications for Cenozoic tectonics, paleogeography, and climate of Asia. *Geological Society of America Special Papers* **507,** SPE507-01 (2014).

56. Caves, J. K. *et al.* Role of the westerlies in Central Asia climate over the Cenozoic. *Earth and Planetary Science Letters* **428,** 33–43 (2015).

57. Yan, Y., Yang, X. & Tang, Z. Patterns of species diversity and phylogenetic structure of vascular plants on the Qinghai-Tibetan Plateau. *Ecology and Evolution* **3,** 4584–4595 (2013).

58. Jacques, F. M. B. *et al.* Quantitative reconstruction of the Late Miocene monsoon climates of southwest China: A case study of the Lincang flora from Yunnan Province. *Palaeogeography, Palaeoclimatology, Palaeoecology* **304,** 318–327 (2011).

59. Ebersbach, J. *et al.* In and out of the Qinghai-Tibet Plateau: divergence time estimation and historical biogeography of the large arctic-alpine genus Saxifraga L. *J. Biogeogr.* **44,** 900–910 (2016).

60. Favre, A. *et al.* Out-of-Tibet: the spatio-temporal evolution of Gentiana (Gentianaceae). *Journal of Biogeography* **43,** 1967–1978 (2016).

61. Favre, A. *et al.* The role of the uplift of the Qinghai-Tibetan Plateau for the evolution of Tibetan biotas. *Biol Rev* **90,** 236–253 (2015).

62. Xing, Y. & Ree, R. H. Uplift-driven diversification in the Hengduan Mountains, a temperate biodiversity hotspot. *PNAS* **114,** E3444–E3451 (2017).

63. Ebersbach, J., Schnitzler, J., Favre, A. & Muellner-Riehl, A. N. Evolutionary radiations in the species-rich mountain genus Saxifraga L. *BMC Evolutionary Biology* **17,** (2017).

64. Ebersbach, J. *et al.* Driving forces behind evolutionary radiations: Saxifraga section Ciliatae (Saxifragaceae) in the region of the Qinghai–Tibet Plateau. *Bot J Linn Soc* **186,** 304–320 (2018).

65. Lei, F., Qu, Y., Song, G., Alström, P. & Fjeldså, J. The potential drivers in forming avian biodiversity hotspots in the East Himalaya-Mountains of Southwest China. *Integrative Zoology* **10,** 171–181 (2014).

66. Barrows, T. T., Stone, J. O., Fifield, L. K. & Cresswell, R. G. Late Pleistocene Glaciation of the Kosciuszko Massif, Snowy Mountains, Australia. *Quaternary Research* **55,** 179–189 (2001).

67. Crisp, M. D., Laffan, S., Linder, H. P. & Monro, A. Endemism in the Australian flora. *Journal of Biogeography* **28,** 183–198 (2001).

68. Japsen, P. *et al.* Episodic burial and exhumation in NE Brazil after opening of the South Atlantic. *Geological Society of America Bulletin* B30515.1 (2012). doi:10.1130/B30515.1

69. Carnaval, A. C., Hickerson, M. J., Haddad, C. F. B., Rodrigues, M. T. & Moritz, C. Stability Predicts Genetic Diversity in the Brazilian Atlantic Forest Hotspot. *Science* **323,** 785–789 (2009).

70. Chaves, A. V., Freitas, G. H. S., Vasconcelos, M. F. & Santos, F. R. Biogeographic patterns, origin and speciation of the endemic birds from eastern Brazilian mountaintops: a review. *Systematics and Biodiversity* **13,** 1–16 (2015).

71. Moucha, R. & Forte, A. M. Changes in African topography driven by mantle convection. *Nature Geoscience* **4,** 707–712 (2011).

72. Kaufmann, G. & Romanov, D. Landscape evolution and glaciation of the Rwenzori Mountains, Uganda: Insights from numerical modeling. *Geomorphology* **138,** 263–275 (2012).

73. Partridge, T. C. & Maud, R. R. Macro-scale geomorphic evolution of southern Africa. in *Macro-scale geomorphic evolution of southern Africa* (eds. Partridge, T. C. & Maud, R. R.) 3–18 (Oxford University Press, 2000).

74. Tinker, J., de Wit, M. & Brown, R. Mesozoic exhumation of the southern Cape, South Africa, quantified using apatite fission track thermochronology. *Tectonophysics* **455,** 77–93 (2008).

75. Scharf, T. E., Codilean, A. T., Wit, M. de, Jansen, J. D. & Kubik, P. W. Strong rocks sustain ancient postorogenic topography in southern Africa. *Geology* **41,** 331–334 (2013).

76. Tyson, P. & Partridge, T. C. The evolution of Cenozoic climates. in *The Cenozoic of Southern Africa* (eds. Partridge, T. C. & Maud, R. R.) 371–387 (Oxford University Press, 2000).

77. Dupont, L. M., Rommerskirchen, F., Mollenhauer, G. & Schefuß, E. Miocene to Pliocene changes in South African hydrology and vegetation in relation to the expansion of C4 plants. *Earth and Planetary Science Letters* **375,** 408–417 (2013).

78. Hoetzel, S., Dupont, L., Schefuß, E., Rommerskirchen, F. & Wefer, G. The role of fire in Miocene to Pliocene C4 grassland and ecosystem evolution. *Nature Geosci* **6,** 1027–1030 (2013).

79. Dupont, L. M., Linder, H. P., Rommerskirchen, F. & Schefuß, E. Climate-driven rampant speciation of the Cape flora. *Journal of Biogeography* **38,** 1059–1068 (2011).

80. Linder, H. P. Plant diversity and endemism in sub-Saharan tropical Africa. *Journal of Biogeography* **28,** 169–182 (2001).

81. Schnitzler, J. *et al.* Causes of Plant Diversification in the Cape Biodiversity Hotspot of South Africa. *Syst Biol* **60,** 343–357 (2011).

82. Linder, H. P., Rabosky, D. L., Antonelli, A., Wüest, R. O. & Ohlemüller, R. Disentangling the influence of climatic and geological changes on species radiations. *J. Biogeogr.* **41,** 1313–1325 (2014).

83. Karger, D. N. *et al.* Climatologies at high resolution for the earth's land surface areas. *Scientific Data* **4,** 170122 (2017).

84. Robinson, N., Regetz, J. & Guralnick, R. P. EarthEnv-DEM90: A nearly-global, void-free, multi-scale smoothed, 90m digital elevation model from fused ASTER and SRTM data. *ISPRS Journal of Photogrammetry and Remote Sensing* **87,** 57–67 (2014).

85. Herman, F. et al. Worldwide acceleration of mountain erosion under a cooling climate. *Nature* **504**, 423–426 (2013).

86. Jarvis, A., Reuter, H. I., Nelson, A. & Guevara, E. SRTM 90m Digital Elevation Database v4.1 | CGIAR-CSI. (2008).

87. New, M., Hulme, M. & Jones, P. Representing Twentieth-Century Space–Time Climate Variability. Part II: Development of 1901–96 Monthly Grids of Terrestrial Surface Climate. *J. Climate* **13,** 2217–2238 (2000).

88. Bookhagen, B. High resolution spatiotemporal distribution of rainfall seasonality and extreme events based on a 12-year TRMM time serie. http://www.geog.ucsb.edu/~bodo/TRMM/ (2013).

89. Hengl, T. *et al.* SoilGrids1km — Global Soil Information Based on Automated Mapping. *PLoS ONE* **9,** e105992 (2014).

90. Willenbring, J. K., Codilean, A. T., McElroy, B. Earth is (mostly) flat: but mountains dominate global denudation: apportionment of the continental mass flux over millennial time scales, revisited. *Earth Surf. Dynam. Discuss.* **2**, 1–17 (2014).